DOI: 10.1002/ejoc.200700805

Thermo-Solvatochromism of Merocyanine Polarity Probes – What Are the Consequences of Increasing Probe Lipophilicity through Annelation?

Clarissa T. Martins,[a] Michelle S. Lima,[a] Erick L. Bastos,[b] and Omar A. El Seoud*[a]

Keywords: Solvatochromism / Thermo-solvatochromism / Merocyanine dyes / Binary solvent mixtures

The question raised in the title has been answered by comparing the solvatochromism of two series of polarity probes, the lipophilicities of which were increased either by increasing the length of an alkyl group (R) attached to a fixed pyridine-based structure or through annelation (i.e., by fusing benzene rings onto a central pyridine-based structure). The following novel solvatochromic probes were synthesized: 2,6-dibromo-4-[(*E*)-2-(1-methylquinolinium-4-yl)ethenyl]-phenolate ($MeQMBr_2$) and 2,6-dibromo-4-[(*E*)-2-(1-methylacridinium-4-yl)ethenyl)]phenolate ($MeAMBr_2$). The solvatochromic behavior of these probes, along with that of 2,6-dibromo-4-[(*E*)-2-(1-methylpyridinium-4-yl)ethenyl]phenolate ($MePMBr_2$) was analyzed in terms of increasing probe lipophilicity, through annelation. Values of the empirical solvent polarity scale [$E_T(MePMBr_2)$] in kcal mol^{-1} correlated linearly with $E_T(30)$, the corresponding values for the extensively employed probe 2,6-diphenyl-4-(2,4,6-triphenylpyridinium-1-yl)phenolate (RB). On the other hand, the nonlinear correlations of $E_T(MeQMBr_2)$ or $E_T(MeAMBr_2)$ with $E_T(30)$ are described by second-order polynomials. Possible reasons for this behavior include: i) self-aggregation of the probe, ii) photoinduced *cis*/*trans* isomerization of the dye, and iii) probe structure- and solvent-dependent contributions of the quinonoid and zwitterionic limiting formulas to the ground and excited states of the probe. We show that mechanisms (i) and (ii) are not operative under the experimental conditions employed; experimental evidence (NMR) and theoretical calculations are presented to support the conjecture that the length of the central ethenylic bond in the dye increases in the order $MeAMBr_2 > MeQMBr_2 > MePMBr_2$. That is, the contribution of the zwitterionic limiting formula predominates for the latter probe, as is also the case for RB, this being the reason for the observed linear correlation between the $E_T(MePMBr_2)$ and the $E_T(30)$ scales. The effect of increasing probe lipophilicity on solvatochromic behavior therefore depends on the strategy employed. Increasing the length of R affects solvatochromism much less than annelation, because the former structural change hardly perturbs the energy of the intramolecular charge-transfer transition responsible for solvatochromism. The thermo-solvatochromic behavior (effect of temperature on solvatochromism) of the three probes was studied in mixtures of water with propanol and/or with DMSO. The solvation model used explicitly considers the presence of three "species" in the system: bulk solution and probe solvation shell [namely, water (W), organic solvent (Solv)], and solvent–water hydrogen-bonded aggregate (Solv-W). For aqueous propanol, the probe is efficiently solvated by Solv-W; the strong interaction of DMSO with W drastically decreases the efficiency of Solv-W in solvating the probe, relative to its precursor solvents. Temperature increases resulted in desolvation of the probes, due to the concomitant reduction in the structured characters of the components of the binary mixtures.

Introduction

The study of solvatochromic substances or polarity indicators (hereafter referred to as "probes") in pure liquids and binary solvent mixtures is important because: **1.** the results obtained shed light on the factors that affect solvation, **2.** the study of thermo-solvatochromism (effect of temperature on solvatochromism) can be used to calculate the energy of desolvation that occurs when the temperature is increased, and **3.** the phenomenon involved in solvatochromism (excitation of the probe ground state) serves as a simple model for other processes.

Recent results have indicated that the molecular structure of the probe and the physicochemical properties of the solvent, or of the binary solvent mixture, are most relevant to solvation (see point **1.** above).[1–6] Although desolvation of reactants and activated complexes contributes to temperature effects on reaction rates, there is no obvious way to calculate this contribution to $\Delta H^{\neq}$ from the Arrhenius plot. This desolvation energy is readily calculated for the probe from its thermo-solvatochromic data (point **2.**). The magnitude of this energy is sizeable relative to the activation enthalpies of many organic reactions (e.g., ranging from 2.1 to 3.7 kcal mol^{-1} over a 50 °C range in aqueous alcohols).[4]

[a] Instituto de Química, Universidade de São Paulo,
C.P. 26077, 05513-970, São Paulo, S.P., Brazil
Fax: +55-11-3091-3874
E-mail: elseoud@iq.usp.br
[b] Centro de Ciências Naturais e Humanas, Fundação Universidade Federal do ABC,
09210-170, Santo André, S.P., Brazil

Supporting information for this article is available on the WWW under http://www.eurjoc.org or from the author.

Examples of point **3.** include the almost identical responses of the rate constants of pH-independent hydrolyses of activated esters (carbonate, chloroformate, and perfluorobutyrate) and of solvatochromic probes to the compositions of binary solvent mixtures.[7,8] More recently, probes of different lipophilicities have successfully been employed to explain the phenomenon of "gelation" of lysozyme solutions in water/tetramethylurea mixtures. Briefly, the enzyme is preferentially solvated by the organic component of the binary mixture; the biomacromolecule/solvent hydrophobic interactions play an important role in the gelation phenomenon.[9] These similar responses to solvent compositions are remarkable because of their distinct origins: attack of water on an acyl group, disruption of the native conformation of an enzyme, and excitation of a ground state of a probe, respectively.

Information is obtained from solvatochromic studies by examining the dependence of an empirical solvent polarity scale [E_T(probe)] defined by Equation (1) on some experimental variable.

$$E_T(\text{probe})\ [\text{kcal mol}^{-1}] = 28591.5/\lambda_{max}\ [\text{nm}] \quad (1)$$

This scale converts the electronic transition within the probe into the corresponding intramolecular charge-transfer transition energy.[1] Examples of some of the probes that we have studied are shown in Figure 1, along with their pK_a (in water) and log P values. The latter refers to the partition coefficient of a substance between (mutually saturated) octan-1-ol and water: $\log P = \log([\text{substance}]_{\text{octan-1-ol}}/[\text{substance}]_{\text{water}})$;[10] hydrophilic and hydrophobic probes are associated with negative and positive log P values, respectively. The probes shown in Figure 1 include 2,6-diphenyl-4-(2,4,6-triphenylpyridinium-1-yl)phenolate (RB), 2,6-dichloro-4-(2,4,6-triphenylpyridinium-1-yl)phenolate (WB), 1-methylquinolinium-8-olate (QB), 4-[(*E*)-2-(1-methylpyridinium-4-yl)ethenyl]phenolate (MePM), and 2,6-dibromo-4-[(*E*)-2-(1-*n*-alkylpyridinium-4-yl)ethenyl]phenolate ($RPMBr_2$; series *SR*; R = methyl to *n*-octyl). The solvent polarity scales of the probes depicted in Figure 1 are referred to as $E_T(30)$, E_T(WB), E_T(QB), E_T(MePM), and $E_T(RPMBr_2)$, respectively.

As shown, RB, WB, and QB differ widely in their molecular structures, and thus in physicochemical properties that are relevant to their solvation. Consequently, quantification of the effects of a single probe property on its solvation (e.g., pK_a or lipophilicity) is not feasible because these properties change simultaneously for each of the probes depicted. A solution to this problem has recently been introduced by examination of the solvatochromism of *SR*, where R = C^1 to C^8. Members of this series differ in their hydrophobic characters, but not in their pK_a values in water. The reason is that the Hammett σ_{para} values for alkyl groups are practically the same,[11] these groups being attached to the pyridinium ring where the negligible differences in their inductive effects are not transmitted to the phenolate oxygen.[5]

An alternative approach to investigation of the effect of the molecular structure of the probe on its solvatochromism is to keep the alkyl group fixed (methyl), while changing the heterocyclic moiety (pyridine, quinoline, and acridine, respectively). The effect of this structural modification would be expected to be different from that observed for *SR*, because fusion of benzene rings onto the heterocyclic ring should change the energies of the resonance hybrids of the ground and excited states. The following compounds were employed: 2,6-dibromo-4-[(*E*)-2-(1-methylpyridinium-4-yl)ethenyl]phenolate ($MePMBr_2$), 2,6-dibromo-4-[(*E*)-2-(1-methylquinolinium-4-yl)ethenyl]phenolate ($MeQMBr_2$), and 2,6-dibromo-4-[(*E*)-2-(1-methylacridinium-4-yl)ethenyl]phenolate ($MeAMBr_2$); see Figure 2 (series *SA*; $MePMBr_2$ is common to both series). The last two probes were synthesized in the present work, whereas $MePMBr_2$ was that studied previously.[5] Although these indicators have close pK_a values in water (the phenolate oxygen of $MePMBr_2$ is 4.2 times more basic than that of $MeAMBr_2$), their lipophilicities are very different ($MePMBr_2$ is 173.8 times more soluble in water than $MeAMBr_2$). A number of

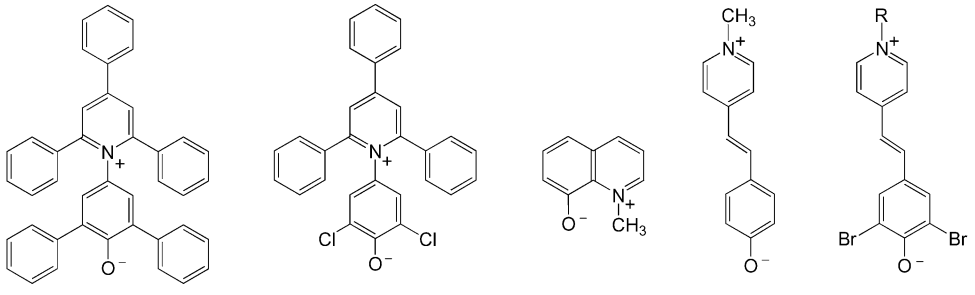

Figure 1. The structures and pK_a (in water) and log P values of some solvatochromic probes.

earlier studies have shown that the electronic structures of merocyanines can be described as resonance hybrids of quinonoid (Q) and zwitterionic (ZW) limiting formulas and that any external perturbation, such as solvation, changes the relative contributions of the limiting formulas to the resonance hybrids of the dyes.[12–14,15]

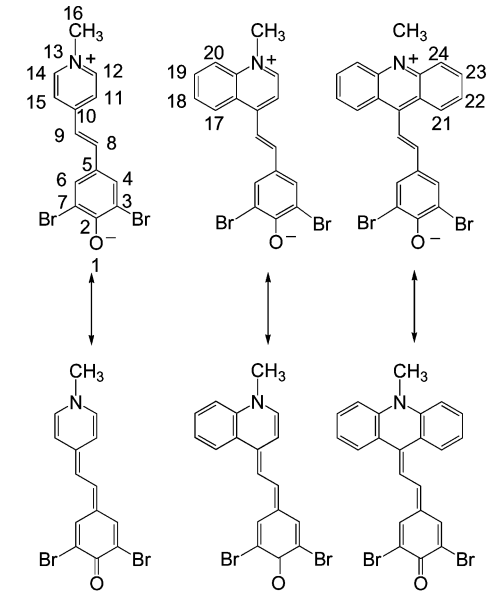

	$MePMBr_2$	$MeQMBr_2$	$MeAMBr_2$
pk_a	5.15	5.03	4.52
log *P*	–0.16	1.02	2.08

Figure 2. Limiting formulas (ZW↔Q), pK_a and log *P* values, and numbering of carbons of the dyes studied.

Solvatochromic responses in thirty-eight protic and aprotic solvents were examined. The correlation of E_T(probe) vs. E_T(30) showed interesting behavior: whereas $E_T(MePMBr_2)$ correlated linearly with E_T(30), a second-degree polynomial was required to describe the same correlation for $E_T(MeQMBr_2)$ and/or $E_T(MeAMBr_2)$, with the latter probe showing positive and negative solvatochromism. Three possible explanations were offered and analyzed. We show that the structure- and solvent-dependent contributions from the two limiting formulas of the probe (ZW and Q) are responsible for the nonlinear correlation. Thermo-solvatochromism was studied at 10, 25, 40, and 60 °C, and at 25, 40, and 60 °C in water/propan-1-ol and water/DMSO, respectively. As a function of increasing temperature, desolvation occurred due to the concomitant decrease of solvent structure; this effect being larger in the case of water/propan-1-ol than in that of water/DMSO.

Results and Discussion

Solvatochromism in Pure Solvents

Values of E_T(probe) in thirty-eight solvents at 25 °C are listed in Table 1.

As shown in part (A) of Figure 3 and in Equation (2), values of $E_T(MePMBr_2)$ correlate linearly with the E_T(30) scale, where *r* and *sd* refer to the correlation coefficient and standard deviation, respectively.[5]

Parts (B) and (C) of Figure 3 show that fusion of one or two benzene rings onto the heterocyclic ring of $MePMBr_2$ results in deviation from linearity; second-degree polynomials are required to correlate $E_T(MeQMBr_2)$ or $E_T(MeAMBr_2)$ with E_T(30), as shown in Equation (3) and Equation (4), respectively, where r^2 is the correlation coefficient. Because of the scatter in Figure 3 (C), and the corresponding r^2 of the regression, Equation (4) is not intended for use for the calculation of $E_T(MeAMBr_2)$ from E_T(30); it just shows that $MeAMBr_2$ exhibits both positive and negative solvatochromism.

Possible explanations for the nonlinear behavior include:
i. aggregation of the more lipophilic probes leading to solvent-dependent formation of dimers and higher aggregates; the measured values of λ_{max} being those of dye monomers or aggregates in solvents of high and low solvent polarity, respectively,[17–23]
ii. the dye undergoing solvent-dependent *cis*/*trans* photoisomerization, with values of λ_{max} being those of the *trans* isomers in polar solvents and their *cis* counterparts in nonpolar ones,[24] and
iii. the transition energy involved (ground state→excited state) essentially reflecting the solvation of the ground state, for which two limiting formulas – zwitterionic and quinonoid – may be written. The contributions of these Lewis structure to the ground states depend on the molecular structures of the dyes, in particular, the number of rings present, and the solvent.[25] These explanations are analyzed below.

1. Auto-Association of the Probes

In assessment of the effects of auto-association on solvatochromic behavior, attention should be paid to the solvent polarity range employed and to the concentration and the molecular structure of the probe, in particular its lipophilicity and propensity to form hydrogen bonds. The linear plot in part A of Figure 3 argues against auto-aggregation of (very lipophilic) RB as the reason for the nonlinear behavior. Nevertheless, the enthalpies of dilution of solutions of RB in some of the alcohols employed in this study (e.g., ethanol, propan-1-ol, butan-1-ol, and octan-1-ol) suggest that this probe aggregates at concentrations greater than 2×10^{-4} mol L^{-1}; Beer's law, however, is obeyed at lower concentrations, less than 2×10^{-5} mol L^{-1}, in cells of 1 cm path length.[17] Since the latter experimental conditions are usually employed, and as we have routinely checked the validity of Beer's law for RB in different solvents, auto-aggregation of that probe can be ruled out; this leaves auto-aggregation of the merocyanine probes as a possible reason. There is spectroscopic evidence (UV/Vis) that some merocyanine dyes, such as 4-[(*E*)-2-(1-hydroxy-*n*-hexylpyridinium-4-yl)ethenyl]phenolate, aggregate in cyclohexane/pyridine mixtures (70:30, v/v) at [probe] $\geq 5 \times 10^{-5}$ mol L^{-1}.[18] This particular probe, however, is prone to aggregation in this

Table 1. Solvent polarity scales [E_T(probe) in kcal mol^{-1}] at 25 °C for $MePMBr_2$, $MeQMBr_2$, $MeAMBr_2$, and RB.[a]

	Solvents	$E_T(MePMBr_2)$[b]	$E_T(MeQMBr_2)$[c]	$E_T(MeAMBr_2)$[c]	$E_T(30)$[d]
1	water	65.24	59.59	50.96	63.1
n-Chain alcohols					
2	methanol	59.24	51.12	41.18	55.4
3	ethanol	56.03	48.36	40.44	51.9
4	propan-1-ol	54.88	47.30	40.11	50.7
5	butan-1-ol	54.15	46.69	40.02	49.7
6	hexan-1-ol	53.07	45.84	39.96	48.8
7	octan-1-ol	52.26	45.32	39.97	48.1
Branched-chain alcohols, other alcohols, 2-alkoxyethanols					
8	propan-2-ol	53.54	46.21	40.14	48.4
9	butan-2-ol	52.29	45.37	40.04	47.1
10	2-methylpropan-2-ol	50.59	43.68	39.97	43.3
11	3-methylbutan-1-ol	53.32	46.05	40.06	49.0
12	ethylene glycol	61.27	52.94	43.51	56.3
13	benzyl alcohol	54.56	47.41	39.67	50.4
14	cyclohexanol	52.50	45.40	39.90	47.2
15	2-methoxyethanol	56.97	48.45	40.40	52.0
16	2-ethoxyethanol	55.52	47.16	40.11	51.0
17	2-propoxyethanol	54.60	46.51	40.03	50.6
18	2-butoxyethanol	54.10	46.12	40.04	50.0
19	2-(2-methoxyethoxy)ethanol	55.42	47.14	40.02	50.6
Chlorinated and aromatic solvents					
20	chloroform	46.12	41.56	40.16	39.1
21	dichloromethane	48.13	42.59	39.95	40.7
22	1,2-dichloroethane	48.55	41.66	40.01	41.3
23	chlorobenzene	–[e]	41.18	44.05	36.8
24	benzene	–[e]	40.82	46.21	34.3
25	toluene	–[e]	40.87	46.36	33.9
26	xylenes	–[e]	–[e]	46.58	34.3
Polar aprotic solvents					
27	acetone	51.06	42.67	40.06	42.2
28	acetonitrile	53.32	44.27	40.54	45.6
29	*N*,*N*-dimethylacetamide	51.98	44.81	40.14	42.9
30	*N*,*N*-dimethylformamide	52.39	45.04	40.04	43.2
31	1,3-dimethylimidazolidin-2-one	51.83	44.72	39.97	42.8
32	DMSO	53.41	45.66	39.78	45.1
33	1,4-dioxane	45.69	41.39	46.39	36.0
34	ethyl acetate	–[e]	42.25	41.72	38.1
35	ethylene glycol dimethyl ether	48.72	42.67	40.90	38.2
36	nitromethane	53.14	46.10	40.14	46.3
37	pyridine	49.66	43.19	40.04	40.5
38	THF	47.69	42.12	40.50	37.4

[a] The uncertainty in E_T(probe) is 0.15 kcal mol^{-1}. [b] Values taken from ref.[5] [c] Values determined in this work. [d] Values taken from ref.[1,16] $E_T(30)$ refers to the empirical polarity scale of the probe RB. [e] Negligible probe solubility precluded measurement of λ_{max}; hence calculation of E_T(probe) in this solvent.

binary solvent mixture of low polarity and relative permittivity ε_r, due to hydrogen bonding between its hydroxy groups, coupled with solvophobic effects.

The plot of E_T(MePM) vs. $E_T(30)$ (see Figure 1) is similar to that shown in Figure 3 (C) (i.e., it shows positive and negative solvatochromism).[12,26] As argued elsewhere, the solvatochromism of this dye is always negative; the positive "branch" of the plot is due to dye aggregation. The reason advanced is that E_T(MePM) values for nonpolar solvents such as chloroform, THF, or 1,4-dioxane were calculated by extrapolation from binary mixtures of these solvents with relatively high concentrations of methanol; this uncertainty in E_T(MePM), together with the high dye concentrations employed, lead to erroneous conclusions (of negative and positive solvatochromism).[26,12]

The key to solving this problem rests on the (chemically plausible) argument that solvents of low ε_r and high viscosity should promote merocyanine aggregation. Almost uniquely, 2-ethylhexan-1-ol possess a large viscosity, 9.8 mPa s at 20 °C, coupled with low ε_r (4.4), so solutions of merocyanines should show aggregation in this solvent. This was experimentally verified for 4-[(*E*)-2-(1-methylnonylpiridinium-4-yl)ethenyl]phenolate in this solvent. At low probe concentration (7.4×10^{-5} mol L^{-1}), the dye shows an intense peak at 575 nm, and a smaller one at 482 nm, attributed to probe monomer, and dimer respectively. Increasing

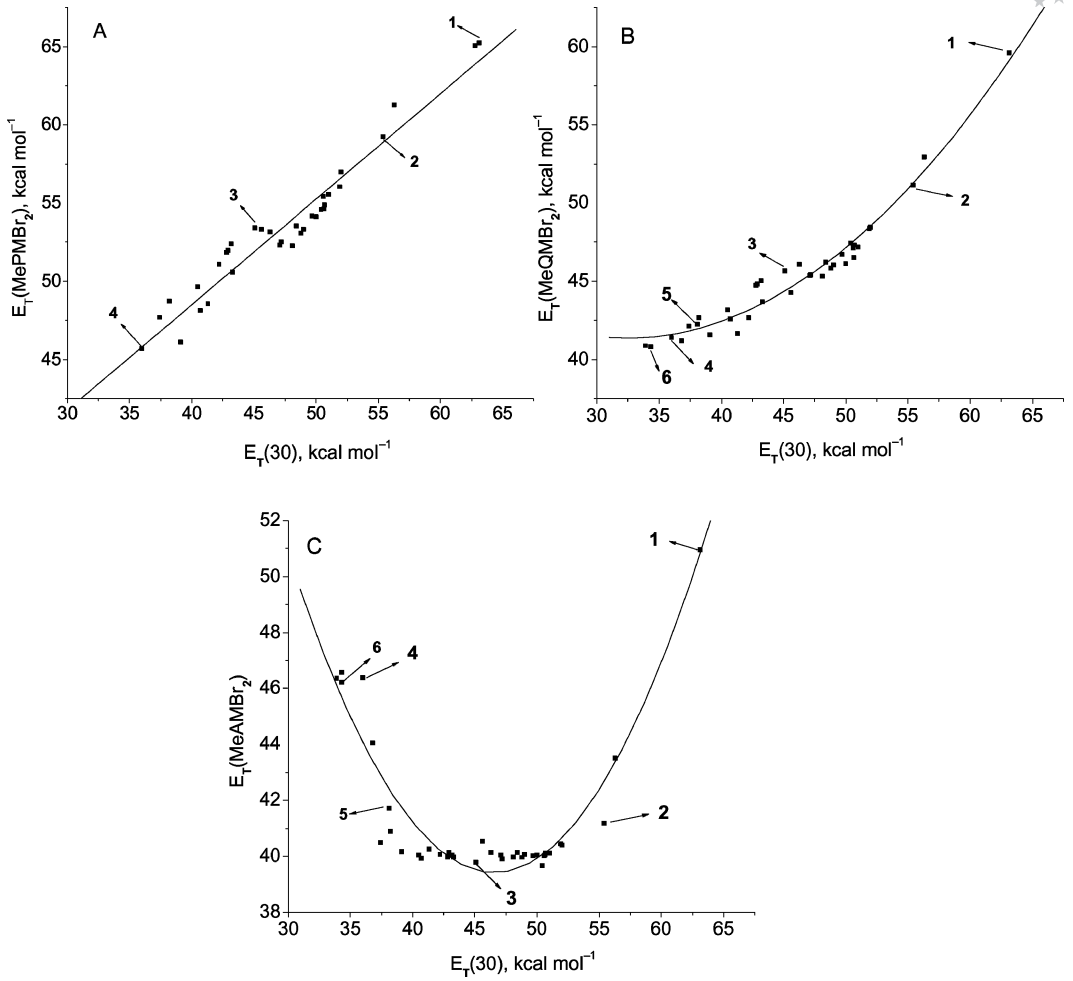

Figure 3. Plots of E_T(probe) vs. E_T(30) for the solvents investigated. The arrows in the graphs refer to: water (1), methanol (2), DMSO (3), 1,4-dioxane (4), ethyl acetate (5), and benzene (6). Note that $MePMBr_2$ is not soluble in the last two solvents.

$$E_T(MePMBr_2) = 10.780 + 0.875\,E_T(30),\ r = 0.9878,\ sd = 0.418 \quad (2)$$

$$E_T(MeQMBr_2) = 61.297 - 1.226\,E_T(30) + 0.019\,E_T(30)^2,\ r^2 = 0.9626,\ sd = 0.731 \quad (3)$$

$$E_T(MeAMBr_2) = 129.854 - 3.885\,E_T(30) + 0.042\,E_T(30)^2,\ r^2 = 0.8990,\ sd = 0.853 \quad (4)$$

the probe concentration to 2.9×10^{-3} mol L^{-1} increased the intensity of the latter peak, at the expense of the former one, and the (overlapped) spectra show a sharp isosbestic point at about 520 nm.[27] This probe, however, is very lipophilic (calculated log P = 4.3;[28] i.e., 166 times more soluble in octan-1-ol than $MeAMBr_2$) and the concentration range is larger than that usually employed in solvatochromic studies; both factors should promote dye auto-aggregation.

The UV/Vis spectra of the employed merocyanines were inspected *as a function of their concentrations* in aprotic and protic solvents (acetone, and ethanol, respectively). No changes in band shapes, or in λ_{max}, and no isosbestic points were observed for the probe concentration ranges listed in Table 2. The same result was observed for solutions of the most lipophilic probe, $MeAMBr_2$, in 2-ethylhexan-1-ol, as shown in Figure S1 in the electronic supporting information. In that case, Beer's Law was obeyed; the absorbance equals 0.155 + 2136.450 [probe], r = 0.9986, *sd* = 0.162. In summary, under the experimental conditions employed, the nonlinear behavior shown in parts B and C of Figure 3 is not due to auto-association either of RB or of the employed merocyanines.

Table 2. Concentration ranges employed to test probe auto-aggregation in different solvents at 25 °C.

Probe	Solvent	Concentration range [mol L^{-1}]
$MePMBr_2$	acetone	1.6×10^{-5} to 2.2×10^{-6}
	ethanol	9.4×10^{-5} to 1.4×10^{-6}
$MeQMBr_2$	acetone	1.3×10^{-5} to 8.1×10^{-7}
	ethanol	5.3×10^{-5} to 2.0×10^{-6}
$MeAMBr_2$	acetone	1.0×10^{-5} to 1.5×10^{-6}
	ethanol	2.4×10^{-5} to 1.5×10^{-6}
	2-ethylhexan-1-ol	2.4×10^{-3} to 4.8×10^{-5}

2. *Thermal or Photoisomerization of cis/trans Forms*

The thermal/photochemical *cis*/*trans* isomerization of merocyanine indicators has been the subject of many studies.[27,29–34] The photochemical/protolytic isomerization cy-

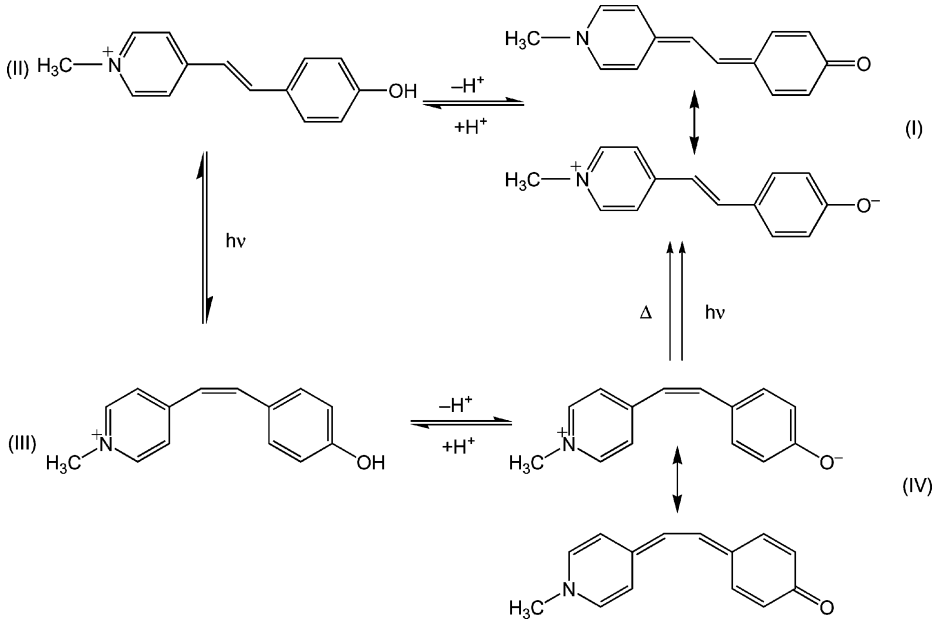

Figure 4. Suggested protolytic/photochemical cycle for MePM.[32]

cle is shown in Figure 4.[32] Protonation of the *trans* isomer (I) produces H^+*trans* (II), which undergoes light-induced isomerization to H^+*cis* (III). This, after deprotonation, produces (IV), which after absorption of light is transformed back into (I); this step is *irreversible*. It is known that the protonated species absorb at lower λ_{max} values than their deprotonated counterparts, due to the disappearance of the CTC band. In this study, (I), (II), and (III) were characterized by ^{1}H NMR spectroscopy. The calculated λ_{max} value for the *cis* isomer (by peak deconvolution) was found to be practically the same as that of its *trans* counterpart, and so (IV), if it were present, would not be detectable by UV/Vis spectroscopy.[33]

cis→*trans* isomerization has been invoked in order to explain the dependence on medium composition of the UV/Vis spectra of another merocyanine probe: 2,6-bis(2-methylpropyl)-4-[(*E*)-2-(1-*n*-dodecylquinolinium-4-yl)ethenyl]phenolate (calculated log *P* = 11.4;[28] apparent pK_a value determined in methanol/water, 70:30, is 7.86).[29] No changes in λ_{max} or spectrum appearance were observed as a function of changing the medium composition (methanol/water), up to 50% water, v/v. In that binary mixture, however, the spectrum appearance changed from two sharp peaks at ca. 625 and 675 nm to a broad band with λ_{max} at ca. 630 nm and with two shoulders at ca. 575 and 725 nm; the intensity of this band decreased as a function of time. Apparently, the probe is (partially) protonated by water at higher water content, followed by (relatively slow) *trans*→*cis* isomerism.[29]

We decided to test whether the probes employed in this study show similar behavior. The UV/Vis spectra of the merocyanines in methanol/water mixtures were examined as a function of the volume fraction of water (0.5 and 0.67, respectively) at 25 and 50 °C, as a function of time (one hour). *In all cases*, the spectra remained the same as a function of time. That is, *trans*→*cis* isomerization does not seem to be operative for any of the probes employed under our experimental conditions.

3. The Nonlinear Correlation is due to Probe Structure- and Solvent-Dependent Contributions of the Quinonoid and Zwitterionic Limiting Formulas to the Ground and Excited States of the Probe

The coupling constants of the hydrogen atoms of the merocyanine ethylenic bonds (i.e., those attached to C^8–C^9) are sensitive to the medium: they decrease as a function of decreasing solvent polarity.[35] Indeed, $J_{H8,H9}$ of MePM decreases in the sequence: 16.12 Hz in [D_4]methanol,[24] 15.20 Hz in [D_6]DMSO,[36] and 14.64 Hz in [D_2]dichloromethane.[24,35] Due to the low solubility of $MePMBr_2$ and $MeQMBr_2$ in $CDCl_3$, we employed 2,6-dibromo-4-[(*E*)-2-(1-octylpyridinium-4-yl)ethenyl]phenolate ($OcPMBr_2$)[5] and 2,6-dibromo-4-[(*E*)-2-(1-butylquinolinium-4-yl)ethenyl]phenolate ($BuQMBr_2$)[37] as models for $MePMBr_2$ and $MeQMBr_2$, respectively. As argued above for *SR*, the length of (R) changes the lipophilicity of the molecule without changing its energy [i.e., without changing the double bond character of the (C^8–C^9) bond]. This assumption can be experimentally tested because the four probes ($MePMBr_2$, $OcPMBr_2$, $MeQMBr_2$, and $BuQMBr_2$) are soluble in [D_6]-DMSO. We found that $J_{H8,H9}$ for *each pair* is the same [i.e., independent of the length of (R)]. ^{1}H NMR spectra of $OcPMBr_2$, $BuQMBr_2$, and $MeAMBr_2$ were recorded in three solvents of decreasing polarity: [D_4]methanol, [D_6]-DMSO, and $CDCl_3$, and the coupling constants are listed in Table 3. For the same probe, values of $J_{H8,H9}$ decrease as a function of decreasing solvent polarity, while for different probes in the same solvent, $J_{H8,H9}$ values decrease as a function of annelation. Reduction of the coupling constant re-

flects a concomitant reduction in the double bond character of (C^8–C^9). In other words, the zwitterionic character of the molecule is reduced as a function of decreasing solvent polarity, and of increasing numbers of benzene rings present.

Table 3. ^{1}H NMR coupling constants (J [Hz]) of the central C^8–C^9 bonds of the probes $OcPMBr_2$, $BuQMBr_2$, and $MeAMBr_2$.

Probe/solvent	Coupling constant, $J_{H8,H9}$ [Hz]		
	$CDCl_3$	[D_6]DMSO	[D_4]Methanol
$OcPMBr_2$	15.0	15.8	15.9
$BuQMBr_2$	13.9	15.0	15.5
$MeAMBr_2$	13.2	13.8	15.0

In conclusion, the nonlinear behavior observed in parts (B) and (C) of Figure 3 is not due to aggregation of any of the probes, cannot be traced to photoinduced *trans*/*cis* isomerization of the conjugate acids, and is consistent with the dependence of $J_{H8,H9}$ on the molecular structure of the probe and the polarity of the solvent. This dependence is due to variable, probe structure- and solvent-dependent contributions of the two limiting formulas (zwitterionic and quinonoid) to the ground and excited states of the probe.

These conclusions are supported by theoretical calculations on the structures and electronic properties of $MePMBr_2$, $MeQMBr_2$, and $MeAMBr_2$. The strategy employed was as follows:

iv. the geometries of all probes were optimized by semiempirical and DFT methods in gas phase and in water by the COSMO treatment,[38]

v. the quality of these optimizations was checked by comparing theoretically calculated bond lengths with experimental ones, where available,

vi. RM1-CI/COSMO and DFT calculations were used to calculate λ_{max} for all probes in the gas phase and water, and

vii. conclusions relating to bond lengths are supplemented by calculations of bond orders by the semiempirical RM1 method.

With regard to points **iv** and **v**, full conformational analysis of the three probes was carried out by molecular mechanics (UFF). Lowest-energy conformers were optimized *without constraints* by the semiempirical RM1 and DFT (B3LYP/6-31+G(d,p)) methods in the gas phase, or in a polarizable water continuum, hereafter referred to as *water*, by the COSMO treatment.[38,39] Figure 5 shows alternative views of optimized structures in the gas phase and in water, predicted by both methods. For additional clarity, alternative views of $MeAMBr_2$ are shown in Figure S2. Tables S1, S2, and S3 in the electronic supporting information show theoretically calculated bond lengths in $MePMBr_2$, $MeQMBr_2$, $MeAMBr_2$, respectively, along with available X-ray data for structurally related compounds.[40,41] Table 4 shows theoretically calculated bond lengths for the central C^8–C^9 bonds in $MePMBr_2$, $MeQMBr_2$, and $MeAMBr_2$.

Table 4. Theoretically calculated bond lengths [Å] for the C^8–C^9 bonds in $MePMBr_2$, $MeQMBr_2$ and $MeAMBr_2$.

	RM1	RM1/COSMO	DFT	DFT/COSMO
$MePMBr_2$	1.426	1.353	1.402	1.371
$MeQMBr_2$	1.430	1.377	1.405	1.377
$MeAMBr_2$	1.447	1.422	1.416	1.389

Both methods predict that $MePMBr_2$ and $MeQMBr_2$ are planar in the gas phase and in water. A nonplanar geometry is predicted for $MeAMBr_2$, presumably in order to reduce H_{C8}–H_{C21} steric interactions (see Figures 2 and 5), in agree-

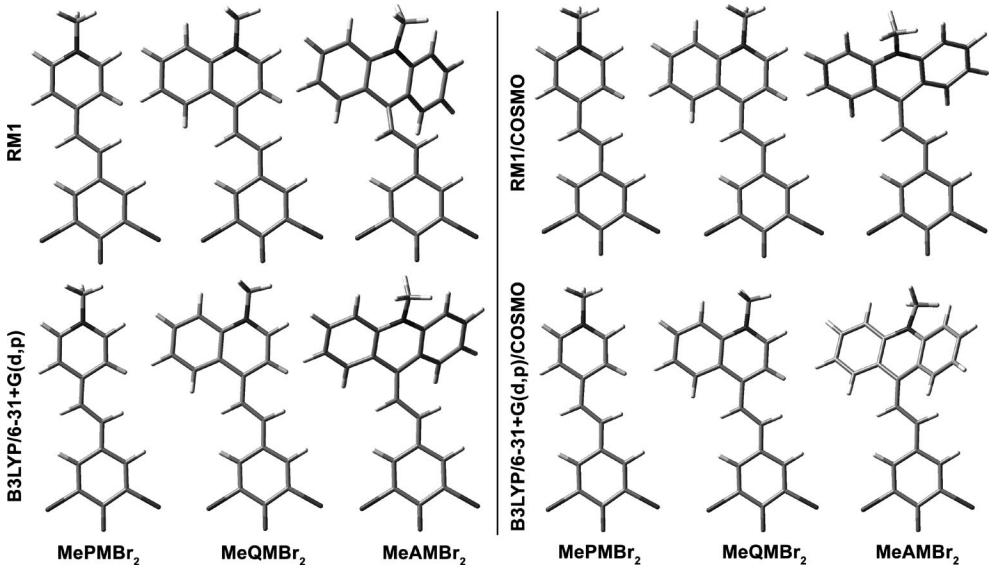

Figure 5. Semiempirical and DFT-optimized geometries of the probes studied in the gas phase and in water.

ment with X-ray data for Me_2ASO_4.[41] The use of the C_s symmetry point group imposes planarity on the acridinium moiety of $MeAMBr_2$. We have also imposed this constraint and repeated the calculation by RM1/COSMO; the energy calculated was found to be 9.2 kJ mol^{-1} higher than that previously calculated (no symmetry constraint, Figure S3).

A comparison of theoretically calculated bond lengths with X-ray-based ones corroborates the correctness of the approach employed. First let us consider $MePMBr_2$ and its precursor MePM. The two bromine atoms in the *ortho* positions in the phenolate moiety of the former probe should affect the O^1–C^2 (*ipso*) bond length significantly. Therefore, it is legitimate to exclude the data relating to this bond from regression analysis. As shown from the *r* values in Table S1, the correlation is poor for gas-phase data ($r \leq 0.67$), but is good for optimization in water ($r > 0.94$), with both methods (RM1 and DFT) giving compatible results. Note that MePM·3 H_2O crystals were employed in the X-ray measurements;[40] this may have contributed to the agreement between data calculated for a compound in water ($MePMBr_2$) and those for a crystal (MePM).

To the best of our knowledge, there are no crystallographic data for any acridine-based merocyanine. Therefore we compared theoretically calculated bonds for the acridinium moiety of $MeAMBr_2$ and the corresponding X-ray-based ones for Me_2AcSO_4; the atom numbering of the latter compound is the same as that employed for the acridinium moiety of $MeAMBr_2$ (Figure 2). For the latter probe, exclusion of the data for C^{10}–C^{11} and C^{10}–C^{15} led to excellent correlations, even for the DFT-based data in the gas phase (Table S3).

Calculated wavelengths (λ_{max}^{calc}) in the gas phase and in water (see **viii.** below) were obtained by performing single-point energy calculations on DFT-optimized geometries of the three probes employed; adiabatic approximation to the time-dependent density functional theory (TDDFT), or the multi-electron configuration interaction (MECI) were employed.[42] In both cases, COSMO was employed to model the water effect; the results are listed in Table 5.

Table 5. Single-point energy calculation of electronic excitation λ_{max}^{calc} [nm] from DFT-optimized geometries and experimentally measured λ_{max}^{exp} [nm] in water.

Probe		RM1-CI	TDDFT
	λ_{max}^{exp} [nm]	λ_{max}^{calc} [nm], difference (%)[a]	
$MePMBr_2$	438.3	497.0 (13)	482.7 (10)
$MeQMBr_2$	479.8	505.4 (5)	534.5 (11)
$MeAMBr_2$	561.1	522.6 (–7)	582.9 (4)
r		0.9999	0.9791

[a] The difference is given by: $(\lambda_{max}^{calc} - \lambda_{max}^{exp})/\lambda_{max}^{exp} \times 100$; *r* refers to the correlation coefficient of plots of λ_{max}^{calc} vs. λ_{max}^{exp}.

The agreements between λ_{max}^{calc} and λ_{max}^{exp} compare favorably with literature data for merocyanine compounds, where differences up to 24% have been reported;[43] significantly, plots of λ_{max}^{exp} vs. λ_{max}^{calc} yielded high *r* values.

For the three probes employed, both RM1-CI and TDDFT indicate the presence of one dominant transition, first dipole-allowed π–π* transition. As shown in Figure 6, the ground states in the *gas phase* show strong quinonoid character (π-bonds in C^5–C^8 and C^9–C^{10} of HOMO), whereas the corresponding excited states have zwitterionic character (π-bonds in C^8–C^9 of LUMO). A different trend is observed for the same probes in water: the characters of the ground and excited states depend on the number of rings present. This can be seen by comparing the C^8–C^9 π-bonds of the HOMOs of $MePMBr_2$ and $MeQMBr_2$ (zwitterionic characters) with the C^5–C^8 and C^9–C^{10} π-bonds of $MeQMBr_2$ (quinonoid characters). In the electronically excited state, $MePMBr_2$ and $MeQMBr_2$ have quinonoid characters, whereas $MeAMBr_2$ is predicted to be mainly zwitterionic (see C^8–C^9 π-bond of the corresponding LUMO).

The above conclusions relating to the characters of the central ethenylic bonds of the dyes can be further corroborated by calculations of the C^8–C^9 bond orders.[35] This ad-

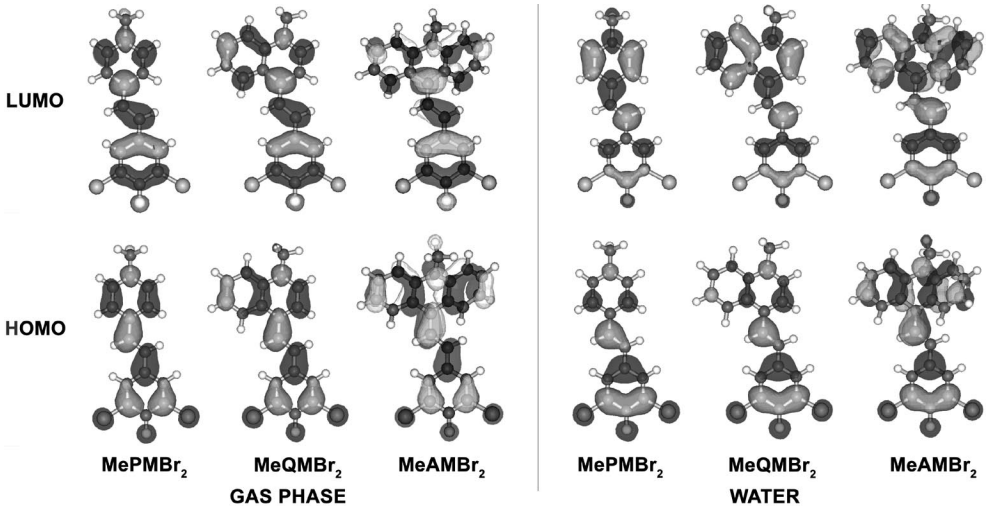

Figure 6. HOMOs and LUMOs of the studied merocyanines calculated in water at the RM1-CI/COSMO level from DFT/COSMO-optimized geometries.

ditional calculation is important because interpretation of the results (in terms of bond character) does not require additional information, such as (unavailable) X-ray data for a model for $MeQMBr_2$. Bond orders both in the gas phase and in water were calculated by single-point calculations in the ground states (S_0, RM1) and the first electronic excited states (S_1, RM1-CI) from DFT-optimized geometries.[35] The results obtained are presented in Scheme 1, where the black bars drawn parallel to the abscissa show the overall change in the calculated orders of the C^8–C^9 bonds; these vary between 1 (single, pure quinonoid) and 2 (double, pure zwitterionic). In the gas phase, all probes show strong quinonoid characters in the ground state (bond orders 1.17, 1.14, and 1.09 for $MePMBr_2$, $MeQMBr_2$, and $MeAMBr_2$, respectively). Excitation from S_0 to S_1 increases their zwitterionic characters, and the magnitude of this change decreases with annelation (bond orders 1.36, 1.32, and 1.26 for $MePMBr_2$, $MeQMBr_2$, and $MeAMBr_2$, respectively). In water, the ground state of $MePMBr_2$ is predicted to have the highest zwitterionic character. On excitation, the order of the C^8–C^9 bond is reduced (from 1.66 to 1.54); the probe is still zwitterionic. The same tendency is observed for $MeQMBr_2$: the reduction in C^8–C^9 bond order is smaller (from 1.59 to 1.56) than that observed for $MePMBr_2$. On the other hand, the order of the C^8–C^9 bond of $MeAMBr_2$ is the smallest among the probes studied, and *increases* on going from the ground to the excited state (from 1.41 to 1.50). That is, the zwitterionic characters of the probes decrease with annelation. This conclusion is in agreement with the dipole moments calculated for the ground and excited states; see Table S4.

In summary, both experimental data (NMR) and the results of theoretical calculations, including bond lengths, bond orders, λ_{max} values, and dipole moments, show that annelation of the basic $MePMBr_2$ structure leads to a decrease in the double bond character of the central ethenylic group in the ground state, and that the solvent-dependence of this change is responsible for the observed inversion of solvatochromism, from negative in polar solvents to positive in nonpolar ones.

Thermo-Solvatochromism in Binary Solvent Mixtures

Thermo-solvatochromism has been studied in propan-1-ol-W and DMSO-W, over the whole composition range, from pure water to pure solvent. The former organic solvent (hereafter referred to as PrOH) is the longest-chain *n*-alcohol that is miscible with water at any ratio; DMSO was chosen because it is a highly dipolar aprotic solvent; it is unique in that DMSO-W interactions are stronger than W-W interactions.[44–48]

Figure 7 shows the dependence of E_T(probe) on solvent composition at 25 °C, for five probes in the two binary mixtures. Our previous results with $BuPMBr_2$ and $OcPMBr_2$ are also included in order to compare the effects of increas-

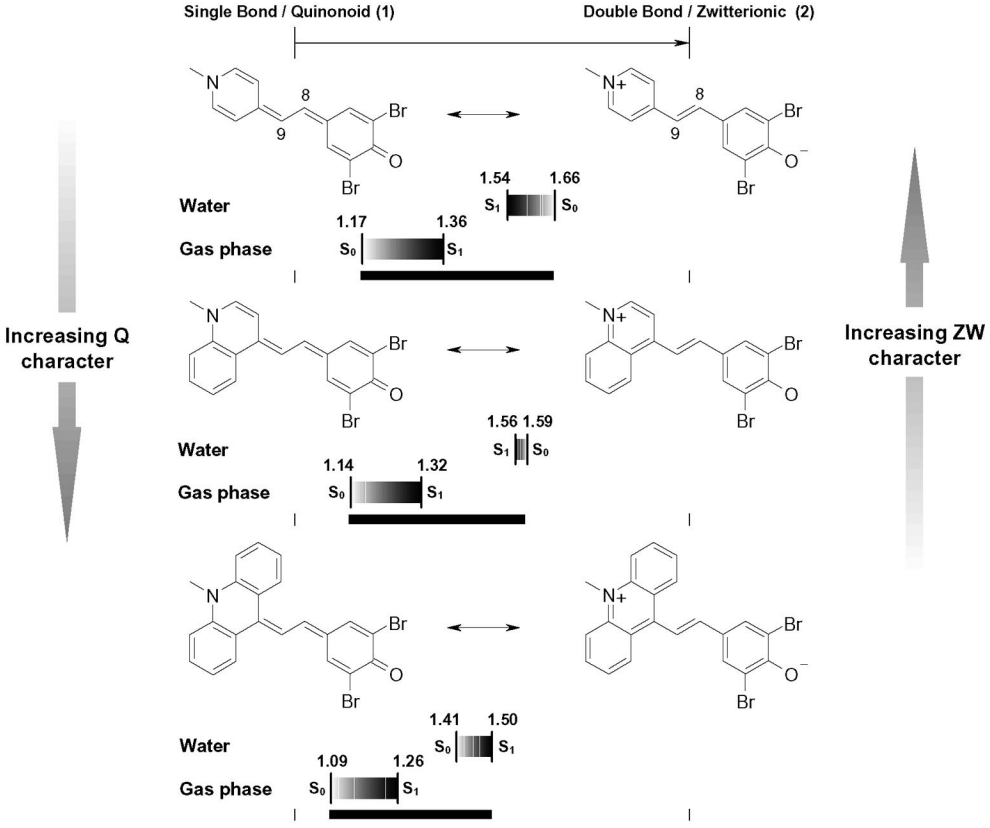

Scheme 1. Bond orders of $MePMBr_2$, $MeQMBr_2$, and $MeAMBr_2$ in water and in the gas phase calculated from RM1//DFT and RM1-CI//DFT, with and without the COSMO treatment.

ing probe lipophilicity, as produced by increasing the length of (R)[5] or by annelation, respectively. All plots are nonlinear (i.e., probe solvation is non-ideal), which may be attributed to several factors and/or solute–solvent interaction mechanisms, as discussed in detail elsewhere.[6] Briefly, the non-ideal behavior may originate from: dielectric enrichment of the probe solvation shell in the solvent of higher relative permittivity ε_r,[49] preferential solvation of the probe by one of the solvent components, or micro-heterogeneity of the binary solvent mixture. The first mechanism can be ruled out, however, because if dielectric enrichment were operative, all curves in Figure 7 should lie above, not below, the straight line that connects the polarities of the two pure liquids. The reason is that the ε_r value for water (73.36) is larger than those for the two organic solvents (20.45 and 46.45 for PrOH and DMSO, respectively).[50] A large body of experimental data and theoretical calculations shows that the binary mixtures employed are micro-heterogeneous: there exist microdomains composed of organic solvent surrounded by water, and of water solvated by organic solvent. The onset and compositions of these microdomains depend on the pair of solvents. There is the possibility of preferential solvation of the (hydrophobic) probe in the less polar microdomains, leading to below the line deviation, as shown in Figure 7.[49,51–53] In summary, non-ideal solvation behavior is not unexpected.

In order to compare the dependencies of E_T(probes) on χ_w, we used Equation (5) to calculate reduced polarity scales.

$$E_T^r = \frac{E_T(\text{aqueous organic solvent}) - E_T(\text{pure organic solvent})}{E_T(\text{water}) - E_T(\text{pure organic solvent})} \quad (5)$$

Figure 7 shows that the effects of increasing probe lipophilicity on its solvatochromic behavior depend on the strategy employed. Values of $\Delta\log P$ are 2.86 and 2.24 for *SR* and *SA*, respectively. That is, although *SR* covers a wider change of lipophilicity, this structural variable has a much smaller impact on solvatochromism than *SA*. The reason for this is that increasing the length of (R) does not perturb the energy of the intramolecular CTC; annelation, on the other hand, has a profound impact on this energy, and hence on solvatochromic response.

The solvent polarity/temperature/solvent composition contours for the three indicators are shown in parts A (PrOH) and B (DMSO) of Figure 8. Considering these results, the following is relevant:

viii. We calculated the (polynomial) dependence of E_T(probe) on the analytical mole fraction of water, and present the regression coefficients in Table S3; E_T(probe) at any χ_W can thus be readily calculated. Note that the degree

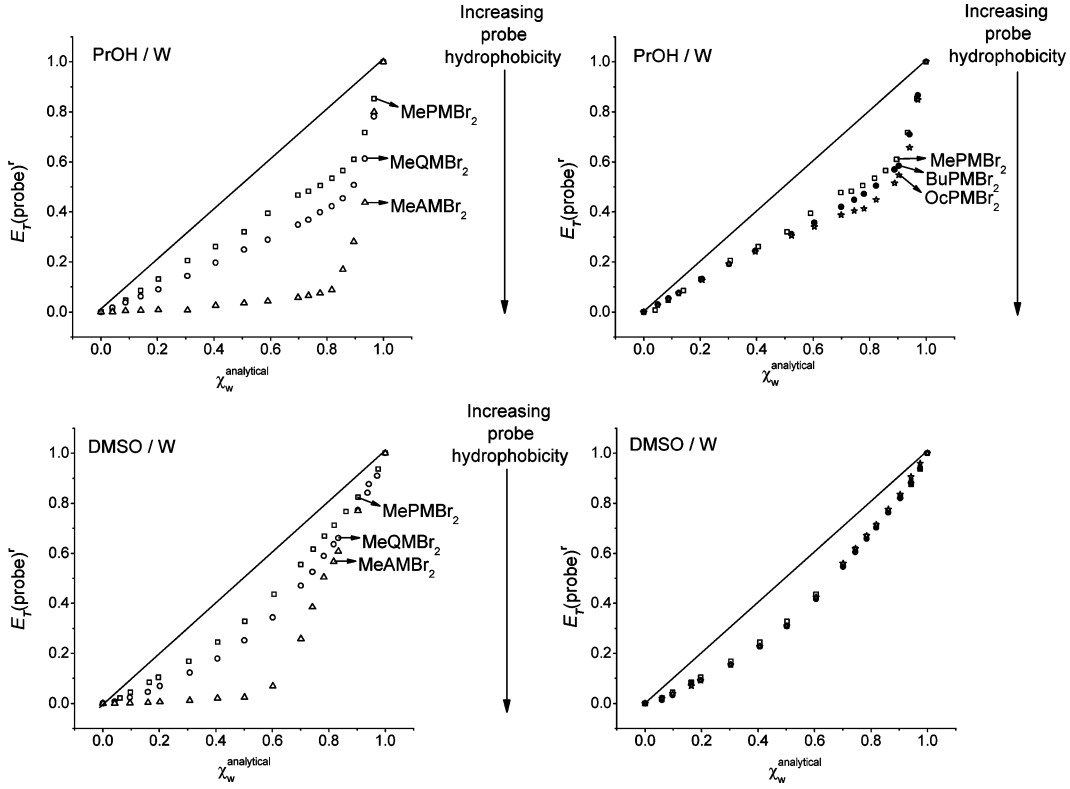

Figure 7. Dependence of the *reduced* empirical solvent polarity parameter [E_T(probe)^r] on the mole fraction of water (χ_W) at 25 °C, for mixtures of water with PrOH and DMSO. The straight lines have been plotted to guide the eye; they represent ideal solvation of the dye by the mixture, see text for details. The probe symbols are: (□) $MePMBr_2$, (○) $MeQMBr_2$, and (Δ) $MeAMBr_2$, (●) $BuPMBr_2$, (*) $OcPMBr_2$.

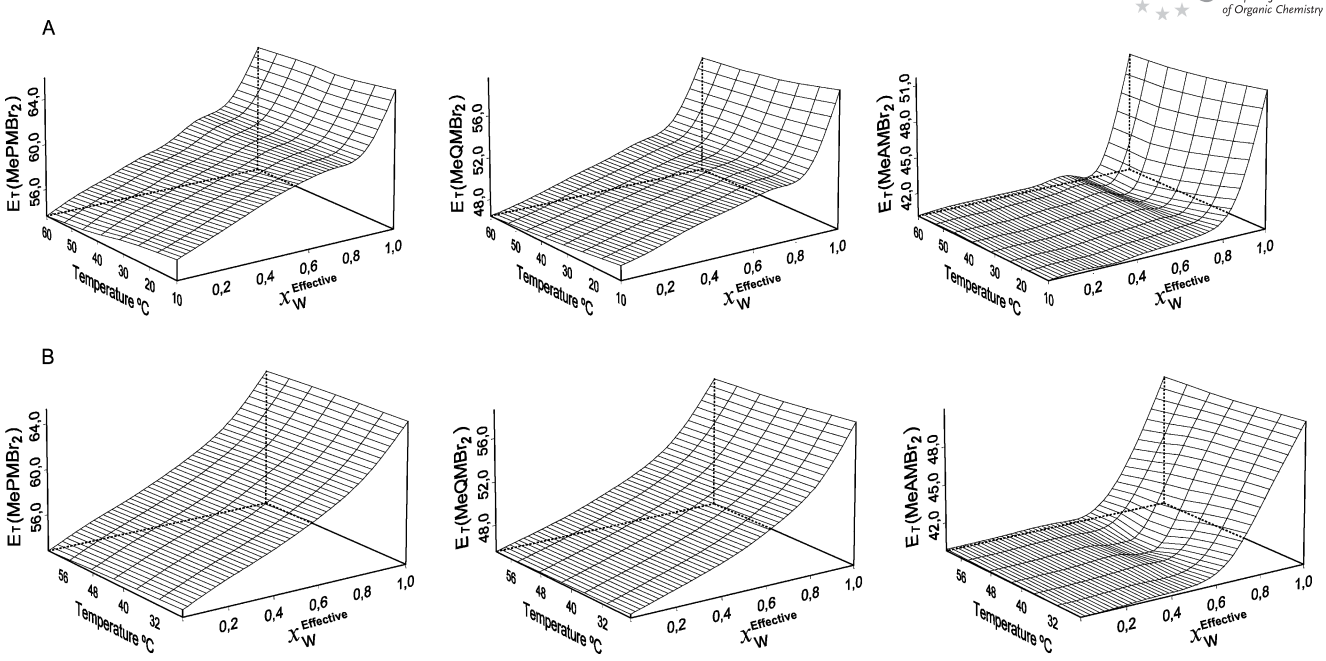

Figure 8. Solvent polarity/temperature/solvent composition contours for $MePMBr_2$, $MeQMBr_2$, and $MeAMBr_2$ in A) PrOH/W, and B) DMSO/W.

of polynomial employed is that which gave the *best* data fit, as indicated by the multiple correlation coefficients r^2 and *sd*. The data for PrOH-W, for example, were conveniently adjusted with a sixth-degree polynomial; for $MePMBr_2$ at 25 °C the corresponding r^2 and *sd* values are 0.9995 and 0.087, respectively. The quality of our data is demonstrated by these statistical criteria and also by the excellent agreement between calculated and experimentally measured $E_T(probe)_{solv}$ values *at all temperatures* (see Table S6).

ix. We treated the data obtained according to the following solvation model, employed in previous studies.[2–4] where (*m*) represents the number of solvent molecules whose exchange in the probe solvation shell affects E_T (usually $m \leq 2$). Arguments for the use of 1:1 stoichiometry for Solv-W have been published elsewhere.[6,54,55] The relevant point in this model is that it *explicitly* considers the formation of hydrogen-bonded (or complex) solvent species Solv-W. Consequently, the mole fractions employed in all calculations (except for those in Table S3) are *"effective" or "local"* (i.e., *not analytical*) ones. The equilibrium constants of Equations (6), (7), and (8) are termed solvent "fractionation factors".

$$\text{Solv} + \text{W} \rightleftharpoons \text{Solv-W} \quad (6)$$

$$\text{Probe(Solv)}_m + m\ \text{(Solv-W)} \rightleftharpoons \text{Probe(Solv-W)}_m + m\ \text{Solv} \quad (7)$$

$$\text{Probe(W)}_m + m\ \text{(Solv-W)} \rightleftharpoons \text{Probe(Solv-W)}_m + m\ \text{W} \quad (8)$$

The superscript Bk refers to bulk solvent. In Equation (9), $\varphi_{W/Solv}$ describes the composition of the probe solvation shell, relative to that of bulk solvent. For $\varphi_{W/Solv} > 1$, the solvation shell is richer in W than bulk solvent, while the converse is true for $\varphi_{W/Solv} < 1$ (i.e., the probe is preferentially solvated by the organic solvent). Finally, a solvent fractionation factor of unity indicates ideal behavior (i.e., the solvation shell and bulk solvent have the same composition). The same line of reasoning applies to $\varphi_{Solv\text{-}W/Solv}$ (complex solvent displaces organic solvent), and $\varphi_{solv\text{-}W/W}$ (complex solvent displaces W), depicted in Equation (10) and Equation (11), respectively.

$$\varphi_{W/Solv} = \frac{x_W^{Probe} / x_{Solv}^{Probe}}{(x_W^{Bk;Effective} / x_{Solv}^{Bk;Effective})^m} \quad (9)$$

$$\varphi_{Solv\text{-}W/Solv} = \frac{x_{Solv\text{-}W}^{Probe} / x_{Solv}^{Probe}}{(x_{Solv\text{-}W}^{Bk;Effective} / x_{Solv}^{Bk;Effective})^m} \quad (10)$$

$$\varphi_{Solv\text{-}W/W} = \frac{x_{Solv\text{-}W}^{Probe} / x_W^{Probe}}{(x_{Solv\text{-}W}^{Bk;Effective} / x_W^{Bk;Effective})^m} \quad (11)$$

x. Results of application of Equations 6 to 8 to the thermo-solvatochromic data for $MePMBr_2$ and $MeQMBr_2$ are listed in Table 6. The data for $MeAMBr_2$ have not been analyzed quantitatively, because they exhibited very pronounced deviation from ideal behavior, as shown in Figure 7. More significantly, $E_T(MeAMBr_2)$ is almost independent of binary mixture composition, up to relatively high water contents. For PrOH-W, the slopes of plots of $E_T(probe)^r$ vs. χ_W, up to χ_W = 0.82 (corresponding to 29.1 mol L^{-1} water) are 0.67, 0.52, and 0.10 for $MePMBr_2$, $MeQMBr_2$, and $MeAMBr_2$, respectively. This indicates that $MeAMBr_2$ is very strongly preferentially solvated by the or-

Table 6. Analysis of thermo-solvatochromic responses of $MePMBr_2$ and $MeQMBr_2$ in solvent/water mixtures, according to Equations 9–11.

Organic solvent	Probe	T [°C]	m	$\varphi_{W/Solv}$	$\varphi_{Solv\text{-}W/Solv}$	$\varphi_{Solv\text{-}W/W}$	$E_T(probe)_{Solv}$	$E_T(probe)_W$	$E_T(probe)_{Solv\text{-}W}$	r^2	χ^2
PrOH	$MePMBr_2$	10	1.580	0.211	71.138	337.147	55.45 [± 0.06]	66 [±0.08]	59.76 [±0.11]	0.9995	0.0069
		25	1.359	0.215	32.546	151.377	54.95 ±0.08	65.42 [±0.11]	59.68 [±0.25]	0.9990	0.0133
		40	1.300	0.233	27.653	118.682	54.34 [±0.09]	65.21 [±0.12]	59.35 [±0.33]	0.9990	0.0142
		60	1.110	0.239	13.105	54.833	53.70 [±0.10]	64.88 [±0.13]	59.60 [±0.70]	0.9989	0.0166
	$MeQMBr_2$	10	1.683	0.129	75.026	581.597	47.89 [± 0.07]	59.55 [±0.11]	51.26 [±0.11]	0.9991	0.0135
		25	1.594	0.144	53.580	372.083	47.44 [± 0.07]	57.80 [±0.10]	51.08 [±0.19]	0.9992	0.0103
		40	1.400	0.158	31.445	199.019	46.97 [± 0.08]	58.02 [±0.11]	50.55 [±0.32]	0.9991	0.013
		60	1.302	0.212	26.522	125.104	46.51 [± 0.07]	57.51 [±0.10]	49.76 [±0.41]	0.9993	0.0102
DMSO	$MePMBr_2$	25	0.768	0.342	0.356	1.041	53.33 [±0.05]	65.25 [±0.06]	57.14 [±7.00]	0.9999	0.0036
		40	0.745	0.412	0.342	0.830	53.12 [±0.03]	65.13 [±0.06]	54.05 [±6.70]	0.9998	0.0044
		60	0.703	0.421	0.242	0.575	52.74 [±0.06]	64.81 [±0.06]	52.93 [±8.25]	0.9998	0.0045
	$MeQMBr_2$	25	0.796	0.287	0.408	1.422	45.82 [±0.05]	58.59 [±0.06]	46.89 [±4.82]	0.9999	0.0037
		40	0.787	0.303	0.401	1.323	45.69 [±0.04]	57.97 [±0.05]	46.25 [±3.75]	0.9999	0.0025
		60	0.783	0.294	0.397	1.350	45.49 [±0.05]	57.46 [±0.06]	45.62 [±4.72]	0.9998	0.0044

ganic component of the mixture; this behavior has not been observed before, even for $OcPMBr_2$, a probe that is more lipophilic than $MeAMBr_2$.[5]

xi. The fit of the model to our thermo-solvatochromic data is shown by values of r^2 and χ^2, and by the excellent agreement between experimentally measured and calculated $E_T(probe)_{solvent}$, and $E_T(probe)_W$ values, respectively. The results in Table 6 are discussed in terms of their dependence on the structures of the probe and the solvent (at the same temperature, T) and on T, for the same probe and solvent. Values of (m) are close to unity, and generally decrease as a function of increasing T. Likewise, for each probe in each solvent, values of $\varphi_{Solv\text{-}W/Solv}$ and $\varphi_{Solv\text{-}W/W}$, $E_T(probe)_{Solv}$, and $E_T(probe)_W$ decrease as a function of increasing T. This probe desolvation is consistent with the known effect of temperature on solvent structure, due to less efficient hydrogen bonding and dipolar interactions.[53]

xii. Values of $\varphi_{W/PrOH}$ are < unity (i.e., water is not efficient in displacing the alcohol from the probe solvation shell). Whereas water and alcohols (ROH) solvate the probe by hydrogen bonding to its phenolate oxygen, PrOH may further interact with the probe through hydrophobic interactions.[5]

xiii. *All* $\varphi_{PrOH\text{-}W/PrOH}$ and $\varphi_{PrOH\text{-}W/W}$ values are >1, indicating that the probes are preferentially solvated by PrOH-W; *all* $\varphi_{PrOH\text{-}W/W}$ values are greater than the corresponding $\varphi_{PrOH\text{-}W/PrOH}$ values, indicating that PrOH-W displaces W more efficiently than PrOH. Since PrOH is more basic than water, we can assume that the structure of the complex species is given by: $\boldsymbol{H}_w$–O–H···O(R)$\boldsymbol{H}_{ROH}$ (i.e., water is the hydrogen bond donor to PrOH, so that the two hydrogen atoms printed in *italics* are the sites for hydrogen bonding with the probe phenolate oxygen). As argued elsewhere, this hydrogen bonding partially deactivates $\boldsymbol{H}_w$ toward further bonding, this deactivation being greater the stronger the basicity of the alcohol.[56,57] Therefore, the efficiency of PrOH-W in displacing alcohol and/or water from the solvation shell does not seem to be due to a better H-bonding ability than those of the pure solvents; it is due to hydrophobic interactions. The order $\varphi_{PrOH\text{-}W/W} > \varphi_{PrOH\text{-}W/PrOH}$ is because $\varphi_{PrOH\text{-}W/W}$ is related to the difference between hydrogen bonding plus hydrophobic interactions of PrOH-W vs. only hydrogen bonding by water, see Equation (8). On the other hand, hydrogen bonding and hydrophobic interactions contribute to solvation by the two solvent species involved in $\varphi_{PrOH\text{-}W/PrOH}$, see Equation (7).[2–4,58,59]

xiv. Solvation by aqueous DMSO is different; whereas $\varphi_{W/DMSO}$ is less than 1 (i.e., similar to solvation by PrOH-W), values of $\varphi_{DMSO\text{-}W/W}$ and $\varphi_{DMSO\text{-}W/DMSO}$ are less than, or close to, unity. To the best of our knowledge, this is the only binary mixture that is inefficient in displacing its precursor components from the probe solvation shell. Consider first the exchange of the pure solvents. Values of $\varphi_{W/DMSO}$ are <1, probably because the organic solvent may solvate the probe through strong dipole–dipole and hydrophobic interactions, akin to those operative in aqueous DMSO.[48] The small magnitudes of $\varphi_{DMSO\text{-}W/W}$ and $\varphi_{DMSO\text{-}W/DMSO}$ may be attributed to the fact that the interaction of DMSO with W attenuates the solvation efficiency of the complex solvent. Several pieces of evidence, including theoretical calculations,[44] IR and ^1H and ^{13}C NMR spectroscopy,[45,46] neutron scattering,[47] and electron-spray mass spectroscopy,[48] have indicated that the DMSO-W interactions are stronger than W-W interactions. Additionally, a plot of a_{mixt} (acidity of the DMSO-W mixtures) vs. χ_{DMSO} shows negative deviation from linearity; the corresponding plot for β_{mixt} (basicity of the DMSO-W mixtures) shows a positive deviation[60] (i.e., aqueous DMSO is less acidic than expected). In other words, DMSO-W aggregate may be regarded as a deactivated species both in hydrogen bonding to the probe phenolate oxygen and in electrostatic interaction with the probe's positively charged nitrogen, which leads to the small φ observed.

xv. Table 6 shows that as a function of increasing temperature, (m), $E_T(probe)_{solv}$, $E_T(probe)_W$, $\varphi_{Solv\text{-}W/solv}$, and $\varphi_{Solv\text{-}W/W}$ decrease, whereas $\varphi_{W/Solv}$ increases (except in one case). The decrease in polarities of pure solvents can be attributed to a decrease in solvent stabilization of the probe ground state, as a result of the concomitant decrease in solvent structure, and hydrogen bonding ability.[61,62] Preferen-

tial "clustering" of water and solvents as a function of increasing temperature means that the strengths of Solv-W interactions *decrease* in the same direction,[52,53,63–66] with a concomitant decrease in ability to displace both water and solvent. This explains the decrease in $\varphi_{Solv\text{-}W/Solv}$ and $\varphi_{Solv\text{-}W/W}$ as a function of increasing *T*.

xvi. The effects of probe lipophilicity on the composition of its solvation shell becomes readily apparent when values of φ are compared (Table 6). For both binary mixtures, at comparable temperatures, *all* $\varphi_{W/Solv}$ values are smaller, and *all* $\varphi_{Solv\text{-}W/Solv}$ and $\varphi_{Solv\text{-}W/W}$ values are larger for $MeQMBr_2$ than the corresponding values for $MePMBr_2$. This dependence on probe structure can be analyzed by considering the solvent/solute interaction mechanisms discussed above; the relative contribution of hydrophobic interactions increases as a function of increasing probe lipophilicity. This leads to less efficient displacement of Solv by W, and more efficient displacement of W and Solv by Solv-W in case of the more lipophilic probe, $MeQMBr_2$.

Conclusions

Solvation in pure solvents is due to interactions that depend on the properties of the solute: namely, structure, pK_a, and lipophilicity, and the solvent. Evaluation of the relative importance of these interactions requires the study of probes of appropriate structures, such as the *SA* and *SR* series. $E_T(MePMBr_2)$ correlates linearly with $E_T(30)$; the nonlinear correlations of $MeQMBr_2$ and $MeAMBr_2$ are due to probe molecular structure- and solvent-dependent contributions of the limiting zwitterionic and quinonoid structures to the corresponding resonance hybrids. This explanation is in agreement with experimentally obtained NMR spectroscopic data and with theoretical calculations of bond lengths, bond orders, and λ_{max}. Thermo-solvatochromism in binary solvent mixtures can be described by a mechanism based on solvent exchange equilibria between the species present in solution (W, Solv, and Solv-W complexes, respectively) and their counterparts in the probe solvation shell. The non-ideal dependence of E_T(probes) on χ_W is mainly due to preferential solvation of the probe, especially by Solv-W; aqueous DMSO is an exception. The temperature effect on φ has been interpreted in terms of the structures of water and solvent and their mutual interactions. Temperature increases result in gradual desolvation of *every* probe, in *all* binary mixtures; desolvation energies depend on the hydrophobicity of the probe and the solvent. A salient point of this study is that the consequences of increasing probe lipophilicity for its solvation depend on the strategy employed in introducing this structural modification. Although the lipophilic character of the *SR* series changes by a factor of 724, plots of E_T(probe) vs. χ_W are similar, showing only progressive dependence on the lipophilicity of the probe. Changing lipophilicity through annelation affects the solvatochromic responses of the three probes noticeably, because this change has a profound impact on the energy of the probe ground and excited states; the latter acquires less zwitterionic character as a function on fusion of benzene rings.

Calculations

Calculation of the Dissociation Constant of Solv-W, K_{dissoc}, $\chi^{Effective}_{Species}$, and Solvent Fractionation Factors

For the solvents studied, K_{dissoc} and $\chi^{Effective}_{Species}$ were available from previous studies.[5] Calculation of these parameters has been discussed in details elsewhere, and will be addressed here only briefly.[2–4] Knowledge of K_{dissoc} (calculated on the basis of dependence of density on the composition of the binary mixture) allows calculation of the effective mole fractions of all solvent species present. The probe solvation micro-sphere is composed of W, Solv, and Solv-W. Observed E_T (E_T^{Obs}) is the sum of the polarity of each component, E_T^W, E_T^{Solv}, $E_T^{Solv\text{-}W}$, respectively, multiplied by the corresponding mole fraction in the probe solvation micro-sphere, χ_W^{Probe}, χ_{Solv}^{Probe} and $\chi_{Solv\text{-}W}^{Probe}$, respectively.

Equations (12) and (13) can then be solved to obtain $E_T^{Solv\text{-}W}$, and the appropriate solvent fractionation factors, respectively.

$$E_T^{obs} = \chi_w^{Probe} E_T^W + \chi_{Solv}^{Probe} E_T^{Solv} + \chi_{Solv\text{-}W}^{Probe} E_T^{Solv\text{-}W} \quad (12)$$

The input data to solve Equation (13) include E_T^{Obs}, E_T^W, E_T^{Solv}, and $\chi^{Effective}_{Species}$, along with initial estimates of (m), $E_T^{Solv\text{-}W}$, and the appropriate φ; values of $\varphi_{Solv\text{-}W/W}$ are obtained by dividing $\varphi_{Solv\text{-}W/Solv}$ by $\varphi_{W/Solv}$.

Experimental Section

Materials: All chemicals were purchased from Acros or Merck. The solvents were purified by the recommended procedures,[67] followed by storing over activated type 4-Å molecular sieves. Their purities were established from their densities (DMA 40 densimeter, Anton Paar, Graz) and from agreement between their experimentally determined $E_T(30)$ and published data.[1,16]

Apparatus: Melting points were determined with an IA 6304 apparatus (Electrothermal, London). Elemental analyses were performed on a Perkin–Elmer 2400 CHN-analyzer (Perkin–Elmer, Wellesley), in the Analytical Center of this Institute. IR and NMR

$$E_T^{obs} = \frac{\left(\chi_{Solv}^{Bk;\,Effective}\right)^m E_T^{Solv} + \varphi_{W/Solv}\left(\chi_W^{Bk;\,Effective}\right)^m E_T^W + \varphi_{Solv\text{-}W/Solv}\left(\chi_{Solv\text{-}W}^{Bk;\,Effective}\right)^m E_T^{Solv\text{-}W}}{\left(\chi_{Solv}^{Bk;\,Effective}\right)^m + \varphi_{W/Solv}\left(\chi_W^{Bk;\,Effective}\right)^m + \varphi_{Solv\text{-}W/Solv}\left(\chi_{Solv\text{-}W}^{Bk;\,Effective}\right)^m} \quad (13)$$

spectra were recorded with a Bruker Victor-22 FTIR spectrometer (Bruker Optics, Ettlingen), and a Varian Innova 300 NMR spectrometer (Varian, Palo Alto). Analysis of the ^{1}H NMR and ^{13}C NMR spectroscopic data was based on simulation of the 1-D spectra, the DQF-COSY, and HETCOR experiments.[68] A vortex mixer (ThermoFischer Scientific, Waltham) or a sonication bath (Laborette 17, Fretsch, Berlin) were employed to accelerate probe dissolution.

Synthesis of the Probes Employed

2,6-Dibromo-4[(*E*)-2-(1-methylquinolinium-4-yl-)ethenyl]phenolate (MeQMBr$_2$): The synthesis of 1,4-dimethylquinolinium iodide was carried out as described previously for MePMBr$_2$.[5] The reaction between methyl iodide and 4-methylquinoline [Equation (14)] was carried out in acetonitrile, followed by removal of the excess of CH_3I and solvent to give a light amber liquid, the purity of which was established by TLC; ethanol/acetic acid/chloroform eluent (1:1:18, by volume). The aldehyde, 3,5-dibromo-4-hydroxybenzaldehyde, was available from a previous study.[37] Condensation of the aldehyde with 1,4-dimethylquinolinium iodide in the presence of piperidine, followed by treatment with KOH [Equation (15)], gave MeQMBr$_2$ as red–purple crystals; these were washed with hot water and dried. Yield 70%, m.p. 270–271 °C. IR (KBr): $\tilde{\nu}$ = 3028 (ν_{C-H}), 1593 ($\nu_{C=C}$), 1213 (ν_{C-N}), 1036 (ν_{C-Br}) cm^{-1}. Calculated for $C_{18}H_{13}Br_2NO$ (%): C 51.58, H 3.13, N 3.34; found C 50.82, H 3.56, N 3.34. The ^{1}H NMR results are given in Table 7.

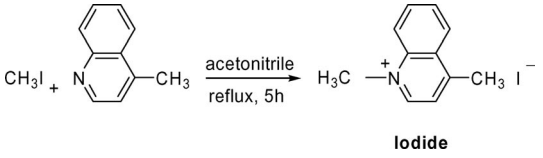

(14)

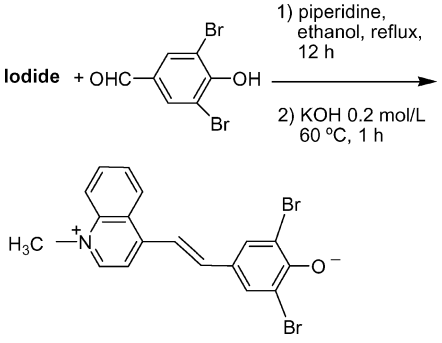

(15)

MeAMBr$_2$ was synthesized as shown in Equations (16) and (17).

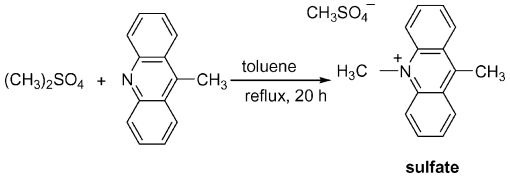

(16)

The synthesis of 9,10-dimethylacridinium sulfate from $(CH_3)_2SO_4$ and 9-methylacridine was carried out as given elsewhere[69] [Equation (16)]. Excess dimethyl sulfate and solvent were removed by distillation, and the yellow product was recrystallized from methanol. Condensation of the methyl sulfate salt with 3,5-dibromo-4-hydroxybenzaldehyde in propan-2-ol, followed by treatment with KOH and recrystallization from methanol [Equation (17)], gave dark greenish-blue crystals, which were washed with water and dried. Yield 70%, decomposes at 209 °C. IR (KBr): $\tilde{\nu}$ = 3034 (ν_{C-H}), 1601 ($\nu_{C=C}$), 1202 (ν_{C-N}), 1044 (ν_{C-Br}) cm^{-1}. Calculated for $C_{22}H_{15}Br_2NO$ (%): C 56.32, H 3.22, N 2.99; found C 55.38, H 2.93, N 2.99. The ^{1}H NMR results are listed in Table 7.

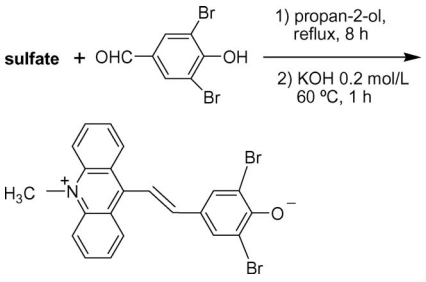

(17)

Spectrometric Determination of log *P*, the Partition Coefficient of the Probe Between Water and Octan-1-ol: The aqueous phase was a phosphate buffer solution (0.05 mol L^{-1}, pH 7.50). Equal volumes of this buffer and octan-1-ol were agitated for one hour (tube rotator), and the phases separated. A probe solution [5×10^{-4} mol L^{-1} in (buffer-saturated) octan-1-ol] was prepared, and its absorbance ($A_{Initial}$) was recorded. An aliquot of this solution ($V_{Octanol}$) was agitated with (octan-1-ol saturated) phosphate buffer (V_{Buffer})

Table 7. ^{1}H NMR spectroscopic data for the probes synthesized: MePMBr$_2$, MeQMBr$_2$, and MeAMBr$_2$.[a]

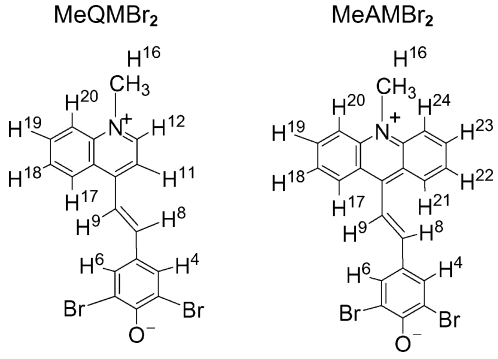

	δ [ppm]	J [Hz]			
H4, H6	8.050 (s)	–	H4, H6	[b]	–
H8	7.591 (d)	$J_{8,9}$ = 15.0	H8	7.668 (d)	$J_{8,9}$ = 13.8
H9	7.998 (d)	–	H9	[b]	–
H11	7.933 (d)	$J_{11,12}$ = 6.9	H17, H21	8.459 (d)[c]	$J_{17,18/21,22}$ = 8.1
H12	8.689 (d)	–	H18, H22	7.477 (m)	–
H17	8.116 (d)	$J_{16,18}$ = 8.4	H19, H23	[b]	–
H18	8.059 (t)	$J_{18,19}$ = 7.5	H20, H24	8.459 (d)[c]	–
H19	7.779 (t)	$J_{19,20}$ = 8.5	H 16	4.025 (s)	–
H20	8.974 (d)	–			
H16	4.238 (s)	–			

[a] At 300 MHz and 25 °C, digital resolution = 0.1 Hz per data point, solvent [D$_6$]DMSO, reference TMS. The following abbreviations were employed for peak multiplicities: d = doublet, m = multiplet, s = singlet, and t = triplet. [b] Chemical shifts are not listed because of peak overlapping (e.g., peak integration of the multiplet at 7.880 to 7.841 ppm corresponds to five hydrogen atoms). [c] These H atoms show the same shifts, peak integration corresponds to five hydrogens.

at room temperature for 6 h. After phase separation at 25 °C, the absorbance ($A_{Equilibrium}$) of the octan-1-ol phase was measured, and the partition coefficient was calculated from: $\log P = \log [A_{Equilibrium} \times V_{Buffer}/(A_{Initial} - A_{Equilibrium}) \times V_{Octanol}]$. Values of $\log P$ were found to be: 1.02 ± 0.01 and 2.08 ± 0.1, for $MeQMBr_2$ and $MeAMBr_2$, respectively.

Spectrometric Determination of the Apparent pK_a Values of the Probes: The pK_a values were calculated from the Henderson–Hasselbach equation.[70] A methanolic probe solution was added to potassium hydrogen phthalate buffer (0.05 mol L^{-1}) so that the final concentration of the probe was 5×10^{-4} mol L^{-1} and the final volume fraction of methanol was ≤ 5%. The concentrations of the probe zwitterionic form were measured at 25 °C, at 480 nm for $MeQMBr_2$ and 562 nm for $MeAMBr_2$. The apparent pK_a values of the probes were found to be 5.03 ± 0.02 and 4.52 ± 0.02 for $MeQMBr_2$ and $MeAMBr_2$, respectively.

Spectroscopic Determination of E_T(Probe) in Pure Solvents and in Binary Solvent Mixtures: Aliquots of the probe solution in acetone were pipetted into 2 mL volumetric tubes, followed by evaporation of the solvent at room temperature, under reduced pressure, over P_4O_{10}. Pure solvents, and/or binary solvent mixtures were added so that the probe final concentration was 10^{-5} to 10^{-6} mol L^{-1}.

A Shimadzu UV 2550 UV/Vis spectrophotometer, was used. The temperature *inside* the thermostatted cell-holder was controlled to within ± 0.05 °C with a digital thermometer (model 4000A, Yellow Springs Instruments, Ohio). Each spectrum was recorded twice at a rate of 140 nm min^{-1}; the values of λ_{max} were determined from the first derivative of the absorption spectra. The uncertainties in $E_T(MePMBr_2)$, $E_T(MeQMBr_2)$, and $E_T(MeAMBr_2)$ are 0.15 kcal mol^{-1}. Thermo-solvatochromism was studied in mixtures, 16 per set, of water with PrOH (from 10 to 60 °C) and DMSO (from 25 to 60 °C). DMSO mixtures were not studied in 10 °C because the pure solvent freezes at this temperature.

Quantum Chemical Calculations: Structures of $MePMBr_2$, $MeQMBr_2$, and $MeAMBr_2$ were optimized by the RM1 semiempirical method, as implemented in MOPAC2007.[39,71] Geometry optimization and vertical excitation energy calculations were performed by the multi-electron configuration interaction (MECI) approach and the RM1 method, hereafter referred to as RM1-CI. The active space was constructed with five molecular orbitals (MOs) and two double-filled levels [C.I. = (5,2), 100 configurations in active space]. Solvent effects on the optical properties were modeled with the conductor-like screening model (COSMO)[38]

Further optimization was performed at the DFT level, with the hybrid B3LYP exchange-correlation functional and the 6-31+G(d,p) basis set as implemented in the Gaussian 03 quantum mechanical package.[72–74]

Vertical excitation energies were calculated from DFT and RM1 geometries with the adiabatic approximation of the TDDFT by use of the B3LYP functional and the 6-31+G(d,p) basis set. All calculations were performed both in gas phase and with the COSMO polarizeable continuum aqueous solvent model coupled to B3LYP/6-31+G(d,p). All geometry optimizations were performed without any constraints, except when otherwise indicated. Stationary points were confirmed as minima via vibrational frequency calculations. Coordinates for optimized geometries are listed in Table S5. All calculations were performed at the advanced computing facilities (LCCA) of the University of São Paulo.

Supporting Information (see also the footnote on the first page of this article): Absorption spectra of $MeAMBr_2$ at different probe concentrations in 2-ethyl-1-hexanol; semi-empirical- and DFT-optimized geometries of $MeAMBr_2$ in the gas phase and in water; RM1-optimized geometry of $MeAMBr_2$ in water, calculated by imposing C_s symmetry point group. Theoretically calculated bond lengths (in Å) for $MePMBr_2$ and crystallographic data of MePM. Theoretically calculated bond lengths (in Å) for $MeQMBr_2$. Theoretically calculated bond lengths (in Å) for $MeAMBr_2$ and crystallographic data of 9,10-dimethylacridinium methyl sulfate, Me_2ASO_4. Dipole moments of the probes in the ground and excited state, calculated by RM1 and RM1-CI methods in water (COSMO). Coordinates for optimized geometries for all the probes studied. Thermo-solvatochromic data for $MePMBr_2$, $MeQMBr_2$ and $MeAMBr_2$ in binary solvent mixtures.

Acknowledgments

We thank the State of São Paulo Research Foundation (FAPESP) for financial support (grant 2004/15400-5), and research fellowships 04/15677-7 and 07/00684-6, to C. T. M. and E. L. B., the National Council for Scientific and Technological Research (CNPq) for a research productivity fellowship to O. A. E. S. (grant 305547/2003-8), and a PIBIC fellowship to M. S. Lima. We also thank Dr. P. A. R. Pires and Mr. C. Guizzo for their help, and the LCCA for making computation facilities available to us.

[1] C. Reichardt, in *Solvents and Solvent Effects in Organic Chemistry*, 3rd ed., VCH, Weinheim, **2003**, p. 389.
[2] E. B. Tada, P. L. Silva, O. A. El Seoud, *J. Phys. Org. Chem.* **2003**, *16*, 691–699.
[3] E. B. Tada, P. L. Silva, O. A. El Seoud, *Phys. Chem. Chem. Phys.* **2003**, *5*, 5378–5385.
[4] E. B. Tada, P. L. Silva, C. Tavares, O. A. El Seoud, *J. Phys. Org. Chem.* **2005**, *18*, 398–407.
[5] C. T. Martins, M. S. Lima, O. A. El Seoud, *J. Org. Chem.* **2006**, *71*, 9068–9079.
[6] O. A. El Seoud, *Pure Appl. Chem.* **2007**, *79*, 1135–1151.
[7] O. A. El Seoud, M. I. El Seoud, J. P. S. Farah, *J. Org. Chem.* **1997**, *62*, 5928–5933.
[8] F. Siviero, O. A. El Seoud, *J. Phys. Org. Chem.* **2006**, *19*, 793–802.
[9] M. A. Silva, C. T. Martins, E. P. G. Arêas, O. A. El Seoud, *Pol. J. Chem.* **2007**, *81*, 1135–1145.
[10] A. J. Leo, C. Hansch, *Perspect. Drug Discovery Des.* **1999**, *17*, 1–25.
[11] C. Hansch, A. J. Leo, R. W. Taft, *Chem. Rev.* **1991**, *91*, 165–195.
[12] H. G. Benson, J. N. Murrell, *J. Chem. Soc. Faraday Trans. 2* **1972**, *68*, 137.
[13] A. Botrel, A. Lebeuze, P. Jacques, H. Strub, *J. Chem. Soc. Faraday Trans. 2* **1984**, *80*, 1235–1252.
[14] E. Buncel, S. Rajagopal, *Acc. Chem. Res.* **1990**, *23*, 226–231.
[15] A. Abbotto, L. Beverina, S. Bradamante, A. Facchetti, C. Klein, G. A. Pagani, M. Redi-Abshiro, R. Wortmann, *Chem. Eur. J.* **2003**, *9*, 1991–2007.
[16] C. Reichardt, in *Solvents and Solvent Effects in Organic Chemistry*, 3rd ed., VCH, Weinheim, **2003**, p. 147.
[17] C. Machado, M. D. Nascimento, M. C. Rezende, A. E. Beezer, *Thermochim. Acta* **1999**, *328*, 155–159.
[18] M. Niedbalska, I. Gruda, *Can. J. Chem.* **1990**, *68*, 691–695.
[19] R. Palepu, H. Gharibi, D. M. Bloor, E. Wynjones, *Langmuir* **1993**, *9*, 110–112.
[20] W. Binanalimbele, R. Zana, *Colloid Polym. Sci.* **1989**, *267*, 440–447.
[21] D. J. Lee, W. H. Huang, *Colloid Polym. Sci.* **1996**, *274*, 160–165.
[22] J. Penfold, E. Staples, I. Tucker, P. Cummins, *J. Colloid Interface Sci.* **1997**, *185*, 424–431.

[23] R. Nagarajan, C. C. Wang, *Langmuir* **2000**, *16*, 5242–5251.
[24] M. Tsukada, Y. Mineo, K. Itoh, *J. Phys. Chem.* **1989**, *93*, 7989–7992.
[25] M. C. Rezende, *J. Braz. Chem. Soc.* **1997**, *8*, 631–635.
[26] P. Jacques, *J. Phys. Chem.* **1986**, *90*, 5535–5539.
[27] J. O. Morley, R. M. Morley, A. L. Fitton, *J. Am. Chem. Soc.* **1998**, *120*, 11479–11488.
[28] *ACD Labs Software*, version V8:19, **1994**–**2006**.
[29] H. Hisamoto, H. Tohma, T. Yamada, K. Yamauchi, D. Siswanta, N. Yoshioka, K. Suzuki, *Anal. Chim. Acta* **1998**, *373*, 271–289.
[30] K. J. Dennis, T. Luong, M. L. Reshwan, M. J. Minch, *J. Phys. Chem.* **1993**, *97*, 8328–8335.
[31] J. Catalan, E. Mena, W. Meutermans, J. Elguero, *J. Phys. Chem.* **1992**, *96*, 3615–3621.
[32] E. Hammam, A. M. El Nahas, *J. Phys. Chem. A* **1998**, *102*, 9739–9744.
[33] U. Steiner, M. H. Abdelkader, P. Fischer, H. E. A. Kramer, *J. Am. Chem. Soc.* **1978**, *100*, 3190–3197.
[34] M. H. Abdelkader, U. Steiner, *J. Chem. Educ.* **1983**, *60*, 160–162.
[35] D. Armstron, P. G. Perkins, J. J. P. Stewart, *J. Chem. Soc. Dalton Trans.* **1973**, 838–840.
[36] E. B. Tada, *Solvatochromism in solvents and in micellar systems*, Ph. D. Thesis, University of São Paulo, São Paulo, **2004**.
[37] C. T. Martins, M. S. Lima, O. A. El Seoud, *J. Phys. Org. Chem.* **2005**, *18*, 1072–1085.
[38] F. Eckert, A. Klamt, *Aiche J.* **2002**, *48*, 369–385.
[39] G. B. Rocha, R. O. Freire, A. M. Simas, J. J. P. Stewart, *J. Comput. Chem.* **2006**, *27*, 1101–1111.
[40] D. J. A. Deridder, D. Heijdenrijk, H. Schenk, R. A. Dommisse, G. L. Lemiere, J. A. Lepoivre, F. A. Alderweireldt, *Acta Crystallogr.* **1990**, *46*, 2197–2199.
[41] J. Meszko, A. Sikorrski, O. M. Huta, A. Konitz, J. Blazejowski, *Acta Crystallogr.* **2002**, *58*, 669–671.
[42] E. Runge, E. K. U. Gross, *Phys. Rev. Lett.* **1984**, *52*, 997–1000.
[43] M. Guillaume, B. Champagne, F. Zutterman, *J. Phys. Chem. A* **2006**, *110*, 13007–13013.
[44] I. A. Borin, M. S. Skaf, *J. Chem. Phys.* **1999**, *110*, 6412–6420.
[45] K. Mizuno, S. Imafuji, T. Ochi, T. Ohta, S. Maeda, *J. Phys. Chem. B* **2000**, *104*, 11001–11005.
[46] S. N. Shashkov, M. A. Kiselev, S. N. Tioutiounnikov, A. M. Kiselev, P. Lesieur, *Physica B* **1999**, *271*, 184–191.
[47] J. T. Cabral, A. Luzar, J. Teixeira, M. C. Bellissent-Funel, *J. Chem. Phys.* **2000**, *113*, 8736–8745.
[48] D. N. Shin, J. W. Wijnen, J. B. F. N. Engberts, A. Wakisaka, *J. Phys. Chem. B* **2001**, *105*, 6759–6762.
[49] P. G. N. Suppan, in *Solvatochromism*, Royal Society of Chemistry, Cambridge, **1997**, pp. 21–67.
[50] D. R. Lide, *CRC Handbook of Chemistry and Physics*, 85th ed., CRC Press, Boca Raton, **2005**.
[51] Y. Marcus, *Chem. Soc. Rev.* **1993**, *22*, 409–416.
[52] I. Shulgin, E. Ruckenstein, *J. Phys. Chem. B* **1999**, *103*, 872–877.
[53] Y. Marcus, *Monatsh. Chem.* **2001**, *132*, 1387–1411.
[54] C. Rafols, M. Roses, E. Bosch, *J. Chem. Soc. Perkin Trans. 2* **1997**, 243–248.
[55] U. Buhvestov, F. Rived, C. Rafols, E. Bosch, M. Roses, *J. Phys. Org. Chem.* **1998**, *11*, 185–192.
[56] B. Kingston, M. C. R. Symons, *J. Chem. Soc. Faraday Trans. 2* **1973**, *69*, 978–992.
[57] M. C. R. Symons, *Pure Appl. Chem.* **1986**, *58*, 1121–1132.
[58] E. B. Tada, L. P. Novaki, O. A. El Seoud, *J. Phys. Org. Chem.* **2000**, *13*, 679–687.
[59] M. S. Antonious, E. B. Tada, O. A. El Seoud, *J. Phys. Org. Chem.* **2002**, *15*, 403–412.
[60] J. Catalan, C. Diaz, F. Garcia-Blanco, *J. Org. Chem.* **2001**, *66*, 5846–5852.
[61] R. Zana, M. J. Eliebari, *J. Phys. Chem.* **1993**, *97*, 11134–11136.
[62] J. R. Haak, J. B. F. N. Engberts, *Recl. Trav. Chim. Pays-Bas* **1986**, *105*, 307–311.
[63] K. R. Harris, P. J. Newitt, *J. Phys. Chem. A* **1999**, *103*, 6508–6513.
[64] K. Nishikawa, H. Hayashi, T. Iijima, *J. Phys. Chem.* **1989**, *93*, 6559–6565.
[65] M. Huelsekopf, R. Ludwig, *J. Mol. Liq.* **2000**, *85*, 105–125.
[66] I. Shulgin, E. Ruckenstein, *J. Phys. Chem. B* **1999**, *103*, 2496–2503.
[67] W. L. F. Armarego, C. L. L. Chai, in *Purification of Laboratory Chemicals*, 5th ed., Elsevier, New York, **2003**, p. 80.
[68] T. D. W. Claridge, in *High Resolution NMR Techniques in Organic Chemistry*, Pergamon, New York, **1999**, p. 148.
[69] C. Huber, K. Fahnrich, C. Krause, T. Werner, *J. Photochem. Photobiol. A* **1999**, *128*, 111–120.
[70] E. V. Anslyn, D. A. Dougherty, in *Modern Physical Organic Chemistry*; University Science Books, Sausalito, **2004**, p. 259.
[71] J. J. P. Stewart, MOPAC2007, version 7.176 W, **2007**.
[72] M. J. Frisch, G. W. Trucks, G. E. Scuseria, M. A. Robb, J. R. Cheeseman, J. Montgomery, Gaussian, Inc., Wallington CT, **2004**.
[73] C. T. Lee, W. T. Yang, R. G. Parr, *Phys. Rev. B* **1988**, *37*, 785–789.
[74] A. D. Becke, *J. Chem. Phys.* **1993**, *98*, 5648–5652.

Received: August 29, 2007
Published Online: January 15, 2008

